A 2D FEM Model For Impedance and Loss Calculation of Armored Three-Core Cables With Inclusion of 3D Pitching Effects

B. Gustavsen, *Fellow, IEEE*

***Abstract*—A method is introduced for impedance and loss calculation of three-core power cables with steel armoring, based on 2D finite element method (FEM) computations. The pitching effect of the cores and armor wires is taken into account by 1) enforcing identical net current on the wires, and by 2) introducing a fictitious non-conductive material between the wires having a complex-valued permeability. The permeability is obtained by considering the effect of the pitching on the total energy in a volume slab around each wire, which involves the solving of a small 2D FEM problem in an optimization loop. The method permits to calculate the positive-sequence and zero-sequence impedance on cables, induced sheath currents, and losses in cores, sheaths, and armor. The method is validated against published results using a full 3D FEM model. The calculations are fast, requiring only a few seconds of computation time. The procedure is simplified by use of pre-calculated look-up tables for the fictitious material permeability value.**

***Index Terms*—Three-core cable, impedance, losses, armor, magnetic, permeability, twisting, pitching, finite element method.**

I. Introduction

THREE-CORE armored power cables are widely applied in offshore wind parks, for in-field collection and for export to shore. Such cables are normally designed as three single core cables inside a common steel wire armoring. The determination of the cable power transfer capability in thermal-electrical analyses requires the ability to correctly calculate the cable power losses on the individual metallic parts. It has been recognized in numerous works [1], [2] that usage of IEC 60287 [3] will for such cables substantially overestimate the losses, which may lead to a non-optimal cable design. The difficulty in modeling three-core armored cables is mainly caused by the pitching (twisting) of the magnetic armor wires in relation to the power cores. The pitching results in the magnetic field getting a low-reluctance component parallel to the wires, in additional to the normal and radial components. This parallel field component causes an enhancement of the field inside the armoring, which increases the induced currents on the metallic sheaths (screens), in addition to modifying the eddy current pattern in the conductors and sheaths. The presence of magnetic steel wires also causes hysteresis losses in addition to eddy-current losses, and these effects are dependent on the pitching steepness. The pitching also causes an even current distribution among the armor wires which must be enforced in calculations.

In the case of armored single-core cables, the wire pitching effect was included in a work by Bianchi and Luano [4]. They introduced a field decomposition approach assuming circular fields which allows to compute an equivalent permeability of a tubular representation of the armor by use of analytical expressions that consider skin effect on conductors. The approach was further developed in [5] by considering axial fields. The works in [4] and [5] are not applicable to three-core cables because 1) the closeness of the power cores leads to uneven current distribution on conductors (proximity effect) which is not accounted for, and 2) because the representation of the wire armor by a tubular conductor will for a three-core armor result in false circulating currents in the armor.

A number of works based on Finite Element Method (FEM) calculation methods have therefore been proposed. Accurate impedance and loss calculation requires in general to use 3D FEM variants which include one effective pitch length of the cable [6], [7], but the resulting calculations are very demanding in CPU time and memory requirements. The computational requirements are greatly reduced by utilizing the problem periodicity by use of boundary conditions [8], which reduces the cable length that needs to be included in the calculation. The accuracy of this model type has been demonstrated to give a good agreement with measurements [9]. The difficulty with long computation times is completely avoided by the use of 2D FEM methods. Although the condition of equal current distribution among armor wires can be enforced in the 2D frame [1], [10], it remains to take into account the field enhancing effects caused by the pitching of the cores and the armor. One way of including the field enhancement effect is by representing the tubular space occupied by the armor with an equivalent non-conductive material [11]. But such approach does not allow to analyze the cable in situations that include zero-sequence current components.

This paper introduces an alternative approach for 2D FEM modeling of power umbilical cables which overcomes the aforementioned limitations. A fictitious material is introduced in the space between the wires that accounts for the magnetic field enhancement, while the wires themselves are explicitly represented. That way, the zero-sequence current components

B. Gustavsen is with SINTEF Energy Research, N-7465 Trondheim, Norway (e-mail: bjorn.gustavsen@sintef.no).

This work was supported by Nexans Norway AS and by NorthWind (Norwegian Research Centre on Wind Energy), www.northwindresearch.no.

can be included in the calculations. The material is non-conductive with a complex-valued permeability that is calculated by considering the effect of the pitching of cores and armor wires on the magnetic energy within a local volume slab around each wire. The condition of equal current distribution among the steel wires is explicitly enforced by a procedure similar to the one in [10]. The model can directly utilize complex-valued permeability obtained from measured B-H curves on steel wires [2], [12]. The resulting method is implemented in a 2D FEM program which permits to calculate the positive-sequence and zero-sequence impedance of three-core power cables in a few seconds, including the induced sheath currents and the losses on individual conductors. Calculated results for a 145 kV 800 mm^2 cable are compared with 3D FEM calculations presented in [13]. One comparison from zero-sequence calculations is also presented. A procedure for simplifying the procedure is shown in Section IX which uses pre-calculated values for the fictitious material permeability. The effects of some adopted simplifications are assessed in the Discussion section.

II. Problem Statement

Consider a three-core power cable as shown in Fig.1. The cable has three cores inside a common round-wire armoring, with each core consisting of a conductor and a metallic sheath. The cores and armor wires are pitched around the cable axis of symmetry, generally with different pitch (lay) lengths.

The objective is to calculate the cable positive and zero-sequence series impedance at the system operating frequency, as well as the induced sheath current and the power losses on the individual metallic parts (cores, sheaths, and armor). The following information is assumed to be available.

1. Geometrical positions, diameters, and conductivities of metallic parts.
2. Pitch length of cores and armor wires.
3. Armor wire permeability.

The calculations are to be performed using 2D FEM while including the (helical) pitching effects of the cores and the armor, including field enhancement, equal current distribution between armor wires, and additional eddy current and hysteresis losses.

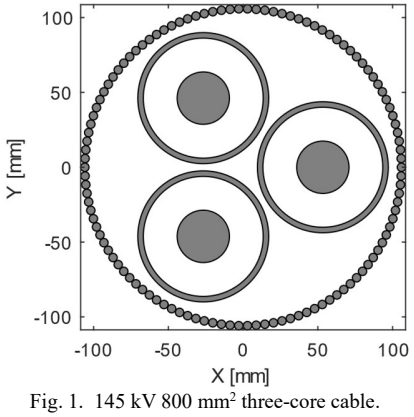

Fig. 1. 145 kV 800 mm^2 three-core cable.

III. Overview of Procedure

The major steps in the modeling procedure are the following.

1. Calculate the permeability μ_* of a fictitious, non-conductive material between armor wires, see Fig. 2.
   i. Define a volume slab around a single armor wire.
   ii. Calculate the fictitious permeability $(\sigma = 0, \mu = \mu_*)$ for the material such that the magnetic field from applied currents in the cable axial direction gives approximately the same magnetic energy in the volume slab as that obtained when considering the effect of the pitching of cores and armor wires.
2. Solve the impedance problem for the complete cable cross-section using 2D FEM.
   i. Introduce the fictitious material between all adjacent wires. (This takes into account the armor field enhancement effects)
   ii. Impose the condition of identical net current on the steel wires. (This prevents false currents from circulating among the wires).
   iii. Solve for impedances, induced currents, and losses.

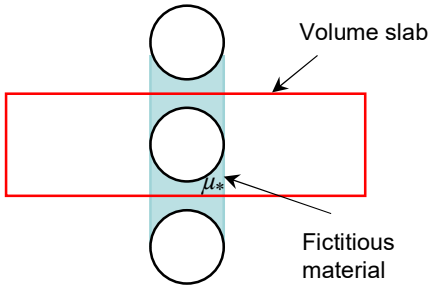

Fig. 2. Introducing a non-conductive fictitious material with permeability μ_* in space between armor wires.

IV. FEM Calculation of Impedances And Losses

A. Two-Dimensional Field Problem

The impedances and losses are obtained by solving the Helmholz equation (1) which considers the magnetic field from an applied current density J_s in the z-direction. A is the z-directional magnetic vector potential with associated magnetic flux density $B = \nabla \times A$, which has components in the x-y plane.

$$\mathrm{div}\left(\frac{1}{\mu}\mathrm{grad}\, A\right) - j\omega\sigma A = -J_s \qquad (1)$$

This 2D field problem is to be modified by an approximate method for including the 3D effects caused by the pitching. This is achieved by 1) enforcing identical net current on the wires (Section V), and by 2) introducing a fictitious complex-valued insulating material between the wires (Section VII).

B. Field Solving And Loss Calculation

The solving of the field problem (1) is in this work performed using the one-step finite element method proposed by Weiss and Scendes [14]. That approach leads to the solving of a linear equation on the form

$$[\mathbf{A}]\begin{bmatrix}\mathbf{a}\\ d\mathbf{v}/dz\\ \hline j\omega\end{bmatrix}=\begin{bmatrix}\mathbf{0}\\ \mathbf{i}\end{bmatrix} \quad (2)$$

where **A** is the system matrix and **i** is a vector of specified currents imposed on conductors, $i_k = J_{s,k}\Delta_k$ where Δ_k is the conductor surface area. The solution vector explicitly contains the voltage drop $d\mathbf{v}/dz$ on these conductors via the relation $J_s = -\sigma \cdot dv/dz$, along with the vector potential **a** on the nodes of the triangular mesh. For an *n*-conductor system, the *n* voltage drops $d\mathbf{v}/dz$ are directly related to elements of the $n \times n$ impedance matrix,

$$-\frac{d\mathbf{v}^{n\times 1}}{dz} = \mathbf{Z}^{n\times n}\,\mathbf{i}^{n\times 1} \quad (3)$$

The power losses on individual conductors are afterwards calculated by integrating the losses over the conductor surface area (4), where J_e is the resulting eddy current density, $J_e = -j\omega\sigma A$.

$$p = \int_S \rho\,|J_s + J_e|^2\,dS \quad (4)$$

The armor losses include hysteresis losses as well as losses in the fictitious, non-conductive material that is to be introduced. The positive-sequence amour losses are calculated indirectly as

$$p_{armor} = 3R_+I_+ - p_{conductors} - p_{sheaths} \quad (5)$$

Further details regarding the actual implementation used in this work are given in [15].

V. Enforcing Identical Currents on Armor Wires

A. Considerations to Current Pattern on Armor Wires

The armor wires follow a helical path around the cable. The following assumptions are made regarding the armor wire currents and voltages.

1. The wire currents follow the helical path of the wires, with negligible current crossing between wires.
2. The induced voltage on each wire is zero over the effective pitch length if the sum of conductor currents and sheath currents is zero.

The above assumptions are consistent with past works.

B. Positive-Sequence Calculation

When calculating Z_+, one applies positive-sequence currents (6) on the power conductors with the condition $dv/dz = 0$ on the metallic sheaths.

$$\mathbf{i}^+ = [1 \quad h^2 \quad h]^T,\ h = e^{j2\pi/3} \quad (6)$$

The symmetrical design of the cable implies that the sum of the sheath currents will be practically zero. The induced voltage on the wires that results from the conductor and sheath currents will therefore be zero, and so the induced wire currents will also be zero. This condition is enforced by specifying zero current on all the wires. The FEM solving returns the voltage drops v_1, v_2, v_3 on the three phase conductors from which the positive-sequence impedance is calculated,

$$Z_+ = [1 \quad h \quad h^2]\cdot[v_1 \quad v_2 \quad v_3]^T/3 \quad (7)$$

The currents and losses on the individual conductors are calculated as outlined in Section IV.Bs.

C. Zero-Sequence Calculation

When calculating Z_0, one applies a zero-sequence current component on the power conductors and again the condition $dv/dz = 0$ on the sheaths. In this case, the induced wire voltages along one wire pitch are non-zero. It is therefore necessary to permit a non-zero current to flow on the wires while at the same time enforcing that the wire currents are identical.

To better explain the proposed method, consider an example where the armor has only four wires. In order to calculate the zero-sequence impedance Z_0, one first calculates the voltage drops dv/dz associated with three separate current applications $\mathbf{i}_1$, $\mathbf{i}_2$, $\mathbf{i}_3$ as shown in Fig. 3. In these calculations, the metallic sheaths are treated as a common conductor such that the system has eight separate conductors. (Because of the symmetry, one can alternatively treat the sheaths as individual conductors with currents $[1/3 \quad 1/3 \quad 1/3]^T$ in $\mathbf{i}_2$.)

	$\mathbf{i}_1$	$\mathbf{i}_2$	$\mathbf{i}_3$		
1	1/3	0	0	Phase conductor	1'
2	1/3	0	0	Phase conductor	
3	1/3	0	0	Phase conductor	
4	0	1	0	Sheaths	2'
5	0	0	1/4	Wire	3'
6	0	0	1/4	Wire	
7	0	0	1/4	Wire	
8	0	0	1/4	Wire	

Fig. 3. Current applications $\mathbf{i}_1$, $\mathbf{i}_2$, $\mathbf{i}_3$, conductors 1-8, and grouped conductors 1', 2', 3'.

Each of the three current applications results in eight voltage drops which are stacked in a matrix $\mathbf{Z}^{8\times 3}$. Next, consider that the conductors are grouped as defined by the rightmost column in Fig. 3. In each current vector, a 1 A current is effectively applied on one group with zero current on the other groups. The voltage drop associated with each group is calculated as the average voltage drop on the individual conductors. The group voltages and currents give together a 3×3 impedance matrix,

$$\mathbf{Z}^{3\times 3} = \begin{bmatrix} 1/3 & 1/3 & 1/3 & 0 & 0 & 0 & 0 & 0\\ 0 & 0 & 0 & 1 & 0 & 0 & 0 & 0\\ 0 & 0 & 0 & 0 & 1/4 & 1/4 & 1/4 & 1/4 \end{bmatrix}\cdot\mathbf{Z}^{8\times 3} \quad (8)$$

where $\mathbf{Z}^{3\times3}$ defines the relation between current and voltage drops on the grouped conductors 1', 2' and 3'. The effect of the ground impedance Z_g external to the FEM solution boundary is added to all elements [15],

$$\mathbf{Z}^{3\times3} \rightarrow \mathbf{Z}^{3\times3} + Z_g \tag{9}$$

If one for instance assumes that the cable is buried in an infinite earth, the impedance Z_g is given by (10) [17] where R is the radius of the FEM solution boundary. K_0 and K_1 are modified Bessel functions of the second kind, of order 0 and 1.

$$z_g = \frac{mK_0(mR)}{2\pi R\sigma K_1(mR)}, \quad m = \sqrt{j\omega\mu\sigma} \tag{10}$$

The equivalent sheath and armor conductors are bonded together by applying the condition $dv_2'/dz = dv_3'/dz$. Simple derivations show that the bonding process leads to a 2×2 matrix which is obtained as

$$\mathbf{Z}^{2\times2} = (\mathbf{P}\cdot(\mathbf{Z}^{3\times3})^{-1}\cdot\mathbf{P}^T)^{-1} \tag{11}$$

with

$$\mathbf{P} = \begin{bmatrix} 1 & 0 & 0 \\ 0 & 1 & 1 \end{bmatrix} \tag{12}$$

Finally, the second row of $\mathbf{Z}^{2\times2}$ is eliminated by specifying $dv/dz = 0$ in the second row-equation. The resulting element is multiplied by three because the current application $\mathbf{i}_1$ in Fig. 3 is one-third of a zero-sequence application. The zero sequence impedance is thus obtained as

$$Z_0 = 3\cdot(Z_{11}^{2\times2} - \frac{Z_{12}^{2\times2}Z_{21}^{2\times2}}{Z_{22}^{2\times2}}) \tag{13}$$

The resulting currents on conductors (total), sheaths (total) and armor (total) are obtained as

$$\begin{bmatrix} i_{\text{conductor}} \\ i_{\text{sheath}} \\ i_{\text{armor}} \end{bmatrix} = -\mathbf{Y}^{3\times3}\cdot\begin{bmatrix} 1 \\ 0 \\ 0 \end{bmatrix}\cdot Z_0\cdot i_{\text{core}} \tag{14}$$

where $\mathbf{Y}^{3\times3} = (\mathbf{Z}^{3\times3})^{-1}$. The obtained current distribution (14) can now be applied as known currents to the conductors if one wishes to analyze the current distribution on individual conductors or power losses. The extension of the method from four to any number of wires is straightforward.

VI. Magnetic Fields

The following describes a procedure for calculating the magnetic field components in the parallel and normal direction on the wires, considering the pitching effect of both cores and armor wires. An effective pitching angle is introduced such that the cores can be considered as straight in the 2D FEM analysis in Section VII, where the fictitious permeability is calculated.

A. Pitching

Three-core cables are designed with a pitching of the cores and armor wires with respect to the cable axial direction. With a pitch length of P_c and P_a for the cores and armor, and mean radius R_a for the armor, we define pitching angles with respect to the armor radius,

$$\alpha = \arctan\frac{2\pi R_a}{P_c} \tag{15a}$$

$$\beta = \arctan\frac{2\pi R_a}{P_a} \tag{15b}$$

B. Positive-Sequence Fields From Cores Pitching

The pitching of the cores results in a modification of the magnetic field components, compared to straight cores. In the following, the effect of the pitching on the field components in the circumferential (ϕ) and axial (z) directions is calculated when the cores are represented by filamentary conductors placed at the core centers. There is also generated a field component in the radial (r) direction but that component will not be considered because it does not have a component parallel to the steel wires.

Consider the current along a helical conductor with pitch P and radius a as shown in Fig. 4. The field components at an observation point (r,ϕ,z) are given by (16a) and (16b) [16]. K_n denotes modified Bessel function of the second kind, and I_n' is the derivative of modified Bessel function of first kind

$$H_\phi = \frac{I}{2\pi r} + \frac{Ia}{2\pi r^2}(kr)F \tag{16a}$$

$$H_z = -\frac{Ia}{2\pi r^2}(kr)^2 F \tag{16b}$$

where

$$F = \sum_{n=1}^{\infty} nI_n'(nka)K_n(nkr)\cos[n(\phi-\phi_0-kz)] \tag{17}$$

$$k = \frac{2\pi r}{p} \tag{18}$$

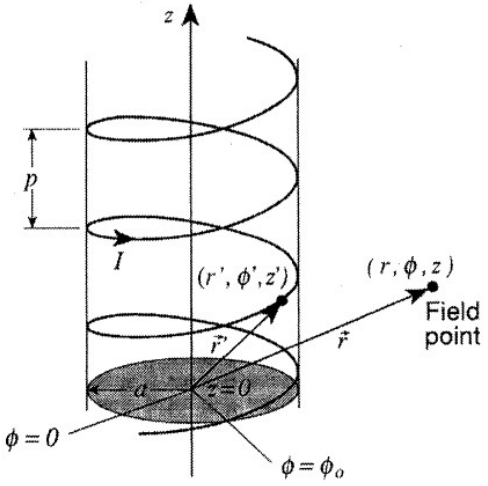

Fig. 4. Line current in helix with pitch P and radius a [16].

The total field from three cores carrying a positive-sequence current is obtained by adding field contributions (16a) and (16b) from three line currents with locations ϕ_i displaced by $(i-1)2\pi/3$, $i=1, 2, 3$.

Consider first the field H' from three straight conductors, giving $H'_z = 0, H'_\phi \neq 0$. (This field can be calculated by (16a) using a sufficiently large value $P >> a$). Next, consider the field H for the helical case, where $H_z \neq 0, H_\phi \neq 0$. In what follows it is shown that the field H in the observation point can be estimated with excellent accuracy from the field H'_ϕ from the straight conductors using (19a) and (19b).

$$H_\phi \approx H'_\phi \cos(\alpha) \tag{19a}$$

$$H_z \approx -H'_\phi \sin(\alpha) \tag{19b}$$

As an example (Table I), consider cores with radial center positions a=53.34 mm, pitching $P_c = 2.8$ m, and observation points on an armor with r=104.5 mm, giving $\alpha = 13.2°$ by (15a). These data correspond to the cable case study in later sections.

TABLE I
GEOMETRY DATA.

	Radial position	Pitch length
Core centers	a=53.34 mm	$P_c = 2.8$ m
Armor wires	r=104 mm	

Fig. 5 shows the magnitude functions of H_ϕ and H_z calculated using either the exact expressions (16a), (16b) or the approximation (19a), (19b). The agreement between the exact and approximate result is excellent. The real and imaginary parts have a similar accuracy (not shown).

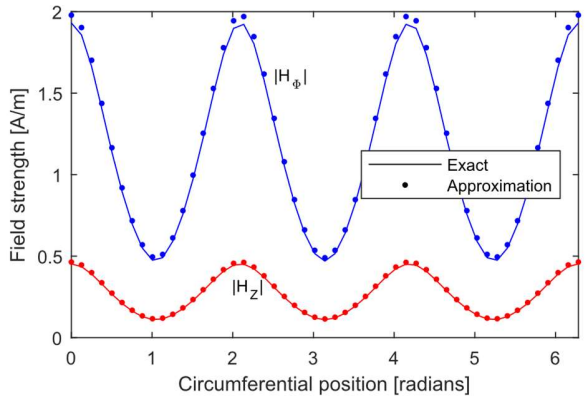

Fig. 5. Field components H_ϕ, H_z from 1 Ampere positive-sequence current application.

C. Positive-Sequence Fields Including Armor Wire Pitching

The magnetic field from the cores gets components that are normal and parallel to the armor wires. Consider the field decomposition to a wire that has a pitching angle β by (15b). Figs. 6a and 6b illustrate the field decomposition of H_ϕ and H_z on the wire, when the wire pitching direction is respectively the opposite and same direction as that of the cores. From the figures and (19a), (19b) it follows that the magnitude of the field components parallel and normal to the wire can be obtained as

$$H^+_{\parallel} = H\sin(\alpha+\beta) = H'_\phi \sin(\alpha+\beta) \tag{20a}$$

$$H^+_{\perp} = H\cos(\alpha+\beta) = H'_\phi \cos(\alpha+\beta) \tag{20b}$$

where the angle of β is negative when pitching directions are the same.

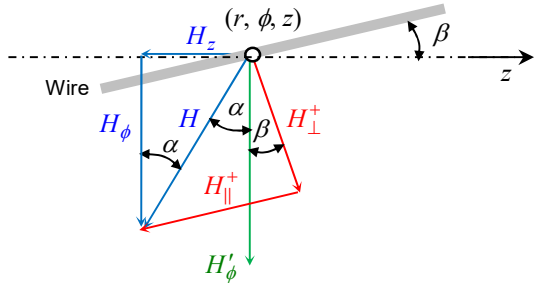

Fig. 6a. Field components $H^+_{\parallel}$ and $H^+_{\perp}$. Pitching in opposite directions.

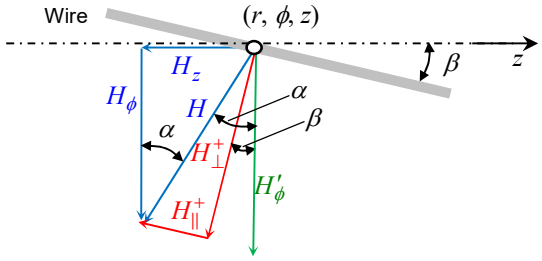

Fig. 6b. Field components $H^+_{\parallel}$ and $H^+_{\perp}$. Pitching in same direction.

D. Zero-Sequence Magnetic Fields From Cores Pitching

Consider now the same example but with a 1 A zero-sequence current applied to the filamentary conductors. Fig. 7 shows the field components H_ϕ and H_z by (16a) and (16b), and an approximation of H_ϕ by H'_ϕ (21). Clearly, the field H'_ϕ from the straight conductors gives an excellent representation of H_ϕ from the helical conductors.

$$H_\phi \approx H'_\phi \tag{21}$$

H_z is seen to be very small compared to H_ϕ. Therefore, the contribution from H_z to the parallel component on a steel wire will also be small. One can therefore conclude that only the pitching of the steel wires needs to be considered in a zero-sequence application when calculating the field components parallel and normal to the steel wires. The estimated values now become

$$H^0_{\parallel} = H'_\phi \sin(\beta) \tag{22a}$$

$$H^0_{\perp} = H'_\phi \cos(\beta) \tag{22b}$$

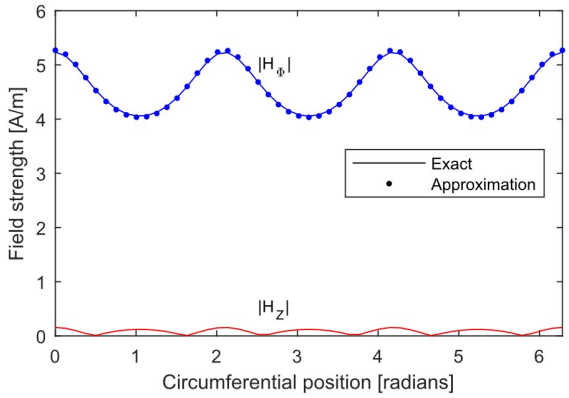

Fig. 7. Field components H_ϕ, H_z from 1 Ampere zero-sequence current.

VII. Including Pitching Effects in 2D FEM Analysis

A. Field Decomposition

The previous section has shown that the field components in the parallel and circumferential directions can be calculated by considering the cores as straight with the armor wires having an effective pitching angle. The effective pitching angle γ is defined by (23a) and (23b) for positive and zero-sequence excitations, respectively. The sign in (23a) is positive for pitching in opposite directions, and negative with pitching in the same direction.

$$\gamma^+ = \alpha + \beta \tag{23a}$$

$$\gamma^0 = \beta \tag{23b}$$

Consider that a positive-sequence or zero-sequence current is applied on the phase conductors. The imposing magnetic field H on an armor wire gets a circumferential component H_ϕ on the wires given by (24) where $\vec{e}_\perp$ and $\vec{e}_{||}$ are unit-length directional vectors.

$$\vec{H}_\phi = \vec{H}_\perp + \vec{H}_{||} = H'_\phi \cos\gamma\ \vec{e}_\perp + H'_\phi \sin\gamma\ \vec{e}_{||} \tag{24}$$

The effect of the field decomposition (24) is in the following two subsections quantified by calculating the associated magnetic energy in the two directions. Finally, a fictitious material is calculated such that the total magnetic energy is preserved in a 2D calculation without fields in the parallel direction. The analysis makes the assumption that the imposed fields $\vec{H}_\perp$ and $\vec{H}_{||}$ are invariant over the slab area.

B. Analysis Domain

We wish to analyze the field in a volume slab that includes the fictitious material in Fig. 2. Due to problem symmetry, it is sufficient to analyze a quarter of the volume slab, as indicated by the shaded area in Fig. 8. The geometry is defined by the wire radius r_w, the gap distance g, and wire permeability μ_w. The slab has height $r_w + g/2$ (circumferential direction), width $r + b$ (radial direction), and depth $r_w + g/2$ (parallel direction). The distance b is chosen sufficiently large to include all field fringing effects in the gap. (In this work, a value $b = 4r_w$ is used while in practice a much smaller distance can be used without noticeably changing the result, e.g. $b = r_w$). The following subsections show that the effect of the parallel field component $H_{||}$ can be included in the normal component $H_\perp$ by introducing an artificial material whose permeability is calculated by requiring the magnetic field energy in the volume slab to be preserved.

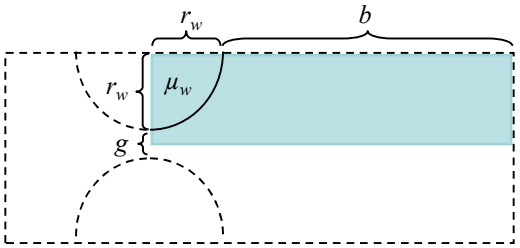

Fig. 8. Volume slab for analysis of field decomposition.

C. Energy Associated With Parallel Field Component

The wire magnetic properties in the parallel direction is assumed to be known from measurements, characterized by a complex permeability $\mu_w^{||}$ that takes into account both eddy current effects (rotational currents) and hysteresis losses. The application of a field strength $H^{||} = 1$ gives an associated energy $W^{||}$ in the volume slab that is calculated analytically by (25). The energy is complex-valued when $\mu_w^{||}$ is complex-valued.

$$\begin{aligned} W_{||} &= \frac{1}{2}\int_V H_{||} B_{||} dV \\ &= \frac{\mu_0}{2}\left[\frac{\mu_{rw}^{||}\pi r^2}{4} + (r_w + b)(r_w + \frac{g}{2}) - \frac{\pi r^2}{4}\right]\cdot(r_w + \frac{g}{2}) \end{aligned} \tag{25}$$

D. Energy Associated With Normal Field Component

The magnetic field associated with an imposed field $H_\perp$ in the normal direction is affected by fringing effects in the air gap which need to be taken into account. Ignoring the effect of eddy currents, the associated 2D field problem is the Poisson equation (26) with a wire permeability $\mu_w^\perp$, where K is a scalar vector field such that $H = -\nabla K$.

$$\mathrm{div}(\mu\,\mathrm{grad}\,K) = 0 \tag{26}$$

Consider the application of a field strength $H_\perp = 1$. The energy $W_\perp$ within the shaded area in Fig. 8 is obtained by solving the scalar field problem (26) in that area using 2D FEM, with boundary conditions given in Fig. 9. The Neumann condition on the left and right boundary forces the *H*-field ($H = -\nabla K$) to become parallel to these boundaries, while the Dirichlet condition on the top and bottom boundary forces the *H*-field to become normal to those boundaries. Moreover, the *H*-field is practically constant along the right boundary. From $H = -\nabla K$ we get $|H| = 1$, which is the same field that was applied in the parallel direction in the preceding sub-section.

The energy $W^{\perp}$ is extracted from the solution by the FEM solver, which for the volume slab is defined by (27). In this work we will use the same wire permeability in the normal and parallel direction, $\mu_w^{\perp} = \mu_w^{\parallel}$.

$$W_{\perp} = \frac{1}{2}\int_V HB dV = \frac{1}{2}(r_w + \frac{g}{2})\int_A HB\, dA \qquad (27)$$

It is to be observed that the field H in (27) is distorted due to field fringing effects. Also, $W_{\perp} < W_{\parallel}$ because the normal field component has a series gap, thereby providing a high-reluctance path for the magnetic flux.

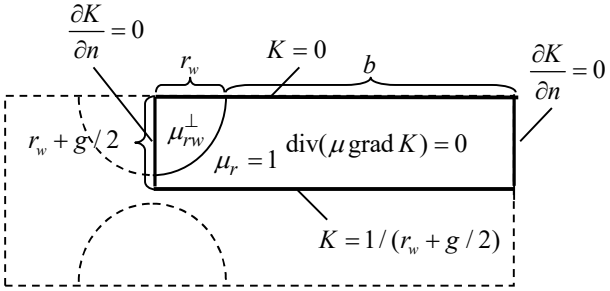

Fig. 9. Field problem for energy calculation, normal field component.

E. Total Energy

The total energy is given by (28) when considering that the imposed field H_{ϕ} has components $H_{\perp} = H'_{\phi}\cos\gamma$ and $H_{\parallel} = H'_{\phi}\sin\gamma$ (24).

$$W_{\mathrm{tot}} = W_{\perp}\cos^2\gamma + W_{\parallel}\sin^2\gamma \qquad (28)$$

F. Representing Total Energy in 2D FEM calculations by Fictitious Material in Wire Gaps

In a 2D FEM computation, there is no parallel field component. In order to include the (increased) energy in the FEM computation, we introduce a *fictitious material* with unknown (complex) relative permeability μ_* and zero conductivity in the space between the armor wires such that $W_{\perp} = W_{\mathrm{tot}}$, see Fig. 10. The permeability μ_* is obtained iteratively by finding the root (zero value) of (29) with $W_{\perp}$ calculated by solving (26) within the rectangular box in Fig. 10.

$$\varepsilon = \min_{\mu_*}(|\, W_{\mathrm{tot}} - W_{\perp}(\mu_*)\cos^2\gamma\,|) \qquad (29)$$

The fictitious material will give field enhancement in both the radial and the circumferential directions. The material should therefore be chosen anisotropic with $\mu_r = \mu_*$ in the circumferential direction and $\mu_r = 1$ in radial direction. However, because the field lines will with normal (small) gap distances tend to follow the low-reluctance path in the circumferential direction, it is permissible to simplify the problem by assuming $\mu_r = \mu_*$ in both directions.

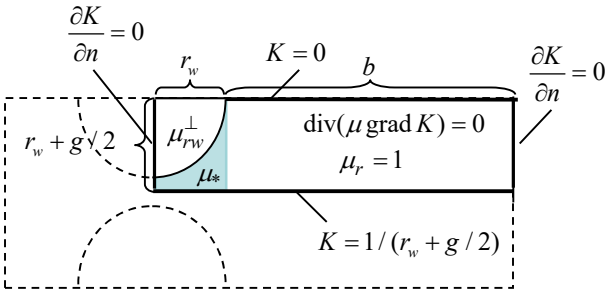

Fig. 10. Introducing non-conductive fictitious material with permeability μ_*.

G. Minimizing Cost Function

The minimization of (29) requires repeated solving of the field problem (26) within the rectangular box in Fig. 9 with two free variables, $\mathrm{Re}\{\mu_*\}$ and $\mathrm{Im}\{\mu_*\}$. The following two-step procedure is used in this work.

1. Find $|\,\mu_*\,|$ such that $|\,\varepsilon\,|$ is minimized, with $\angle\mu_*$ fixed.
2. Find $\angle\mu_*$ such that $|\,\angle\varepsilon\,|$ is minimized, with $|\,\mu_*\,|$ fixed.

Both steps 1 and 2 involve finding the minimum of a concave function and is therefore fast. The procedure starts with $\angle\mu_* = 0$. Suitable bounds are specified for $|\,\mu_*\,|$ and $\angle\mu_*$. Steps 1-2 are performed two times, requiring less than 2 seconds of CPU time.

VIII. Comparison Against 3D FEM Calculations

The modeling accuracy is in the following assessed for an 145 kV 800 mm^2 three-core armored cable by comparing calculated results against those by a 3D FEM program [13]. Additional information about the geometry and the calculated results were provided by one of the authors of [13], Prof. Juan Carlos del Pino López.

A. Cable Geometry and Material Parameters

The cable geometry and material properties are defined in Fig. 1 and Table II. There exists a small 0.16 mm gap between the wires. The three cores have a pitch (lay) length of 2.8 m while two alternative pitch lengths are considered for the armor: 4.5 m and 2 m, with pitching in opposite direction of the cores.

TABLE II
CABLE PARAMETERS.

Item	Parameter	Value	Unit
Conductor	Radius	17.5	mm
	Conductivity @20 °C	$48.23\cdot10^6$	S/m
	Thermal coefficient	0.00393	°C^{-1}
Sheath	Radius, outside	43.8	mm
	Thickness	3.7	mm
	Conductivity @20 °C	$4.7\cdot10^6$	S/m
	Thermal coefficient, α	0.004	°C^{-1}
Armor	Outside diameter	214.6	mm
	Number of wires	114	
	Wire diameter	5.6	mm
	Conductivity @20 °C	$7.3\cdot10^6$	S/m
	Thermal coefficient, α	0.0045	°C^{-1}
	Permeability	300-*j*50	

TABLE III
PITCHING.

Item	Pitch length, P	α , β
Cores	2.8 m (positive direction)	13.2°
Armor wires	4.5 m or 2.0 m (negative direction)	8.3° or 18.2°

B. Parameter Conversion

In order to compare with calculated results by the 3D FEM model, some parameter conversions are necessary.

1) Armor Permeability

The permeability listed in Table II ($\mu_r = 300 - j50$) was in the 3D FEM calculations [13] used as a material constant, i.e. it was used along with the steel wire conductivity. This implies that the permeability imaginary part is intended to account for hysteresis losses only. In the proposed work (this paper), the permeability in the parallel direction $\mu_w^{\parallel}$ is assumed to account for both eddy current losses and hysteresis losses. A parameter conversion process is therefore applied which calculates a modified permeability where the effect of the conductivity is included, see Appendix. Note that the modified permeability is only used for calculating the fictitious permeability μ_* whereas the original permeability ($\mu_{rw} = 300 - j50$) is used in the 2D FEM calculation of the complete problem (1) where the wire conductivity is non-zero, $\sigma = \sigma_{Fe}$.

2) Conductivities

The 3D FEM model was in [13] applied in a thermal-electrical analysis, resulting in different temperatures on the metallic parts (conductors, sheaths, armor). The conductivities in Table II are accordingly modified by (30), using the average temperatures on the conductors from the 3D FEM calculations together with the thermal coefficients α from Table III. The average temperatures are listed in Table IV, for the two armor pitch lengths used in the following subsections.

$$\sigma(T) = \frac{\sigma(T_{20})}{1 + \alpha(T - T_{20})} \tag{30}$$

TABLE IV
AVERAGE TEMPERATURE ON CONDUCTORS.

	Temperature T		
Armor pitch length	Phase conductors	Sheaths	Armor
4.5 m	67.3 °C	59.6 °C	48.3 °C
2.0 m	70.1 °C	62.2 °C	51.1 °C

C. Positive-Sequence Excitation Results

In the first comparison, the armor pitch length is 4.5 m, giving an effective pitch angle $\gamma = 21.5°$ by (23a). A 50 Hz positive-sequence current of 732 A is applied to the phase conductors, with the sheaths and armor grounded.

The first row in Table V shows the calculated results by the 3D FEM model [13]. The next four rows show the deviation from the 3D result by three alternative 2D FEM models. Models M2 and M3 do *not* include the fictitious material.

- M1: 2D FEM model proposed in this work.
- M2: 2D FEM model with enforcement of identical current on all armor wires.
- M3: 2D FEM model where currents are allowed to circulate among the (bonded) armor wires.

The proposed model (M1) is seen to give an excellent agreement with the result by the 3D model, for series impedance (R_+, X_+), induced sheath currents, and power losses in phase conductors, sheaths and armor. Use of M2 and M3 gives much higher errors. With both methods (M2, M3), the missing field enhancement gives too low sheath currents, and the sheath losses are therefore too small. The conductor and sheath losses are also affected by proximity effects, which are different for the three models (M1, M2, M3) due to differences in the magnetic field strength and its distribution inside the armor. Use of M3 also gives much too high armor losses due to false circulating currents among the armor wires.

The permeability of the artificial material used by M1 is $\mu_{r*} = 2.89 - j1.30$. Fig. 8 shows the scalar magnetic potential K by solving (19).

TABLE V
RESULT BY 3D FEM AND PER CENT ERRORS BY 2D FEM MODEL ALTERNATIVES. $P_c = 2.8$ m, $P_a = 4.5$ m, $I_+ = 732$ A.

	R_+ [Ω]	X_+ [Ω]	I_{sheath} [A]	P_{cond} [W/m]	P_{sheath} [W/m]	P_{armor} [W/m]
3D FEM	0.0501	0.122	158.9	50.0	25.7	4.8
M1 err %	**-1.0**	**-0.2**	**2.0**	**-2.7**	**-0.1**	**11.9**
M2 err %	-12.0	-2.1	-5.0	-3.3	-14.5	-88.3
M3 err %	-8.0	-8.1	-16.3	-5.1	-34.2	103.8

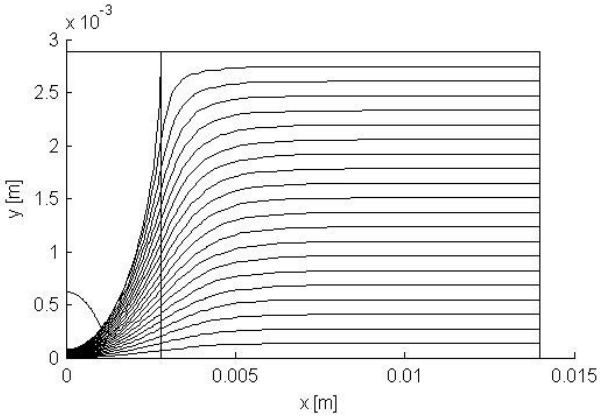

Fig. 11. Magnetic scalar potential (K) in solution area.

Table VI shows the same result when the armor pitch length is reduced to 2.0 m such that the effective pitch angle is $\gamma = 31.4°$. The proposed model (M1) still gives a good agreement with the 3D FEM model. The armor losses are now 16.7% too high, but this amounts to only 0.8 W/m which is insignificant compared to the total losses (84.8 W/m). The errors by models M2 and M3 are generally higher than for the previous case with 4.5 m armor pitch length. The permeability of the artificial material is $\mu_{r*} = 5.49 - j3.08$.

TABLE VI
RESULT BY 3D FEM AND PER CENT ERRORS BY 2D FEM MODEL ALTERNATIVES. $P_c = 2.8$ m, $P_a = 2.0$ m, $I_+ = 732$ A.

	R_+ [Ω]	X_+ [Ω]	I_{sheath} [A]	P_{cond} [W/m]	P_{sheath} [W/m]	P_{armor} [W/m]
3D FEM	0.0528	0.125	167.2	50.8	29.0	5.0
M1 err %	**-1.2**	**-0.7**	**1.1**	**-2.4**	**-2.0**	**16.7**
M2 err %	-16.2	-4.1	-10.3	-4.4	-24.6	-88.4
M3 err %	-13.4	-9.6	-20.5	-5.6	-41.5	71.1

D. Zero-Sequence Impedance

A comparison with 3D FEM was made for the zero-sequence impedance $Z_0 = R + jX_0$. The temperature on power conductors, sheaths and armor are 68 °C, 60 °C and 51 °C, respectively, and the sea conductivity is 5 S/m. The cores and armor pitch lengths are $P_c = 2.8$ m and $P_a = 3.5$ m, with pitching in opposite directions.

Table VII shows the calculated result by 3D FEM, and the deviation from this solution by models M1, M2 and M3. It is observed that all three models give a good agreement with the 3D FEM result, with the result by M1 marginally less accurate than that of M2 and M3. The difference in the result by models M1, M2 and M3 is much smaller than with the positive-sequence calculations.

TABLE VII
ZERO-SEQUENCE IMPEDANCE. $P_c = 2.8$ m, $P_a = 3.5$ m.

	$P_c = 2.8$ m, $P_a = 3.5$ m	
	R_0 [Ω]	X_0 [Ω]
3D FEM	0.16701	0.12972
M1 dev%	1.5%	-1.6%
M2 dev%	-1.0%	-0.5%
M3 dev%	-1.0%	-0.6%

E. CPU Times

The calculations were performed using a 155 368 element triangular mesh. The ensuing calculation of the impedances, induced currents, and losses required 17 sec on a 2.8 GHz dual core desktop computer. Using a coarser mesh with 39 232 triangles gave practically the same result, but within 3.2 sec.

IX. SIMPLIFIED CALCULATION ASSUMING REAL-VALUED WIRE PERMEABILITY

Often, the information about the armor wire permeability is given by a real-valued quantity μ_w. The effective permeability μ_{eff} considering eddy current effects can still be calculated by the approach in Section B in Appendix when assuming $\mu_{mat} = \mu_w$, leading to a complex-valued permeability. The procedure can be further simplified by simply setting $\mu_{eff} = \mu_w$. With this assumption, the permeability μ_* of the fictitious material becomes real-valued, and it depends only on the ratio g / d_w between the wire gap distance g and the wire diameter $d_w = 2r_w$, in addition to the effective pitching angle γ and the permeability value μ_w.

Fig. 12a shows the calculated value for $\mu_* - 1$ as function of γ, with $g / d_w = 0.01$. It is observed that the permeability μ_* to be used increases with increasing values for γ and μ_w. It follows that look-up tables can be easily generated for various combinations of g / d_w, γ and μ_w. That way, 2D FEM modeling can be easily used for impedance and loss calculations. Figs. 12b and 12c show the corresponding results for two alternative values 0.02 and 0.03 for g / d_w.

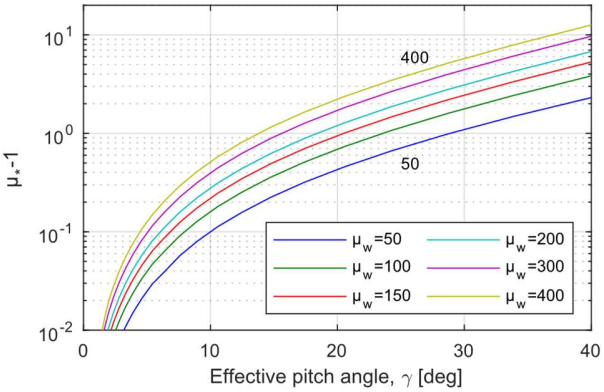

Fig. 12a. Permeability of fictitious material. $g / d_w = 0.01$.

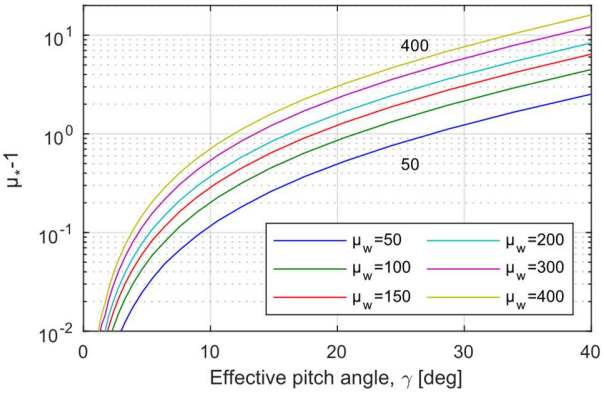

Fig. 12b. Permeability of fictitious material. $g / d_w = 0.02$.

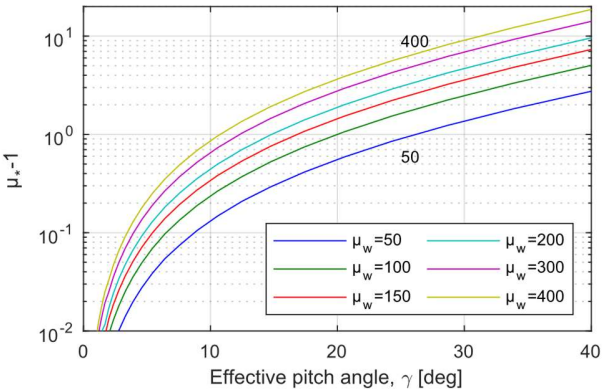

Fig. 12c. Permeability of fictitious material. $g / d_w = 0.03$.

Table VIII shows with bold characters the calculated positive-sequence quantities, when using a real-valued

permeability $r_w = \sqrt{300^2 + 50^2} = 304$ for the case with 2.0 m armor pitch length. With $g / d_w = 0.0285$, this gave $\mu_* = 8.6$ for the fictitious material. The accuracy is lower than for the original model M1 (Table VI), but still substantially more accurate than the results by M2 and M3.

TABLE VIII
RESULT BY 3D FEM AND PER CENT ERRORS BY 2D FEM SIMPLIFIED MODEL. $P_c = 2.8$ m , $P_a = 2.0$ m .

	R_+ [Ω]	X_+ [Ω]	I_{sheath} [A]	P_{cond} [W/m]	P_{sheath} [W/m]	P_{armor} [W/m]
3D FEM	0.0528	0.125	167.2	50.8	29.0	5.0
M1 dev%	-2.0	1.1	4.7	-2.0	4.5	-40.5

X. DISCUSSION

A. Representation of Magnetic Field Distribution

The pitching of cores and armoring leads to a magnetic field distribution that is not correctly represented in the solution by standard 2D FEM calculations because the conductors are here assumed to be straight. This work has shown how to approximately take into account the pitching effects on electrical parameters by introducing a non-conductive, magnetic material between the armor wires, which intends to take into account the field components that result parallel to the armor wires. It is to be noted that the procedure is only an approximation. E.g., it does not consider the increase in magnetic energy in the space between the cores and armor that is associated with the axial, solenoid-like field caused by the cores pitching.

B. Impact of Proximity Effects on Modeling Assumptions

One specific simplification being made is the use of core centers as locations for the equivalent filamentary current when calculating the effect of the pitching on the field component parallel to the wires. In reality, the proximity effects causes a displacement of the radial position a in (16a), (16b) and (17). With a positive-sequence current excitation, the displacement is such that a is reduced on the power conductors and increased on the sheath conductors. The relative shift is in general dependent on the conductor sizes and the frequency of the applied currents.

C. Comparison With 3D FEM Results

Despite the approximations being made, the resulting method was shown in Section VIII to give an excellent reproduction of calculated positive-sequence parameters (impedance, induced sheath currents, total losses) for an 800 mm^2 cable when compared to a full 3D FEM solution, with errors smaller that 2%. The accuracy is much better compared to the result by a plain 2D FEM calculation, with or without enforcement of equal current on the armor wires. One validation was made for the zero-sequence result. Here, a good result was obtained for all 2D FEM variants.

D. Simplified Variant

Section IX proposes a simplified variant using real-valued permeability for the steel wires, which leads to a real-valued permeability μ_* for the fictitious material. This approach was shown to give a slightly reduced accuracy for positive-sequence parameters than the one using a complex permeability. Nevertheless, the accuracy was found to be substantially higher than for alternative 2D approaches, including enforcement of equal wire currents (M2) and bonded wires (M3). Look-up values for μ_* were presented in Figs. 12a, 12b and 12c that can be used for determining the fictitious material, without having to resort to the more sophisticated approach in Section VII. The permeability values are dependent on the ratio between gap distance and wire diameter, and not on the wire diameter itself. Therefore, the presented μ_* values are applicable for any three-core cable with single-layer armoring.

E. Further Work

The method in this work is intended for modeling three-core cables with a single-layer steel armoring having a small gap distance between the wires. Further developments and validations should be performed for this geometry and other geometries, e.g. two-layer armors, and armors with a wide gap between the wires.

XI. CONCLUSION

A 2D finite element model is proposed for calculating the positive and zero-sequence impedance parameters of armored three-core cables featuring a single-layer steel armor. The model takes into account the pitching (twisting) effect of cores and armor wires by introducing a fictitious non-conductive material between the wires with permeability μ_*, in addition to enforcing identical currents on the wires. That way, the magnetic field enhancement effects and additional losses caused by the pitching are accounted for. Comparison with calculated results by a full 3D model demonstrates good accuracy for positive-sequence parameters: impedance, induced sheath currents and loss distribution on conductors. The model should be attractive for practicing engineers because 1) it can be applied using widely available 2D FEM programs, and 2) the calculation time is very short (a few seconds). The use of the method is simplified by use of precalculated look-up tables for μ_*. The accuracy of the approach should be assessed also for zero-sequence parameters as well as other cable designs, e.g. three-core cables with two-layer armors, and armors with a wide separation between the wires.

APPENDIX A - PERMEABILITY CONVERSIONS

A. Permeability Representations

The wire permeability is treated as a material constant μ_{mat} in the complete 2D FEM model (Section IV), i.e. with $\sigma = \sigma_{Fe}$. But the calculation of the parallel and normal field components with associated energies (Section VII) requires the use of an effective permeability μ_{eff}, i.e. with $\sigma \approx 0$. Therefore, two alternative permeability representations μ_{mat} and μ_{eff} are

needed.

B. Conversion From μ_{mat} to μ_{eff}

Consider the (parallel) magnetic field created by a unit length current sheet around a wire with radius r_w. The associated impedance is given by (31) [21], where I_0 and I_1 are modified Bessel functions of the first kind.

$$Z = j\omega L_0 \frac{2I_1(m r_w)}{m r_w I_0(m r_w)},\ L_0 = \mu_r \mu_0 \pi r_w^2,\ m = \sqrt{j\omega \mu_r \mu_0 \sigma} \quad (31)$$

A reference impedance is calculated by (31) using $\mu = \mu_{mat}$ and the actual steel conductivity, $\sigma = \sigma_{Fe}$. The effective permeability μ_{eff} is next calculated by numerical optimization where the conductivity is set to a low value (32). The solving is done in two stages. The magnitude of μ_{eff} is first modified so that the error in $|Z(\mu_{eff})|$ becomes zero, and the angle of μ_{eff} is next modified such that the error of $\angle Z(\mu_{eff})$ becomes zero. The two-step procedure is repeated until convergence. The procedure resulted in that the permeability $\mu_{mat} = 300 - j50$ in Section VII was converted to $\mu_{eff} = 173 - j128$.

$$\varepsilon = \min_{\mu_{eff}} (Z(\mu_{eff}, \sigma \approx 0) - Z(\mu_{mat}, \sigma = \sigma_{\mathrm{Fe}})) \quad (32)$$

C. Conversion From μ_{eff} to μ_{mat}

The opposite situation is that the permeability is given as the effective permeability μ_{eff}, e.g. when obtained from B-H measurements on representative steel wires. The material constant μ_{mat} is easily calculated using a very similar procedure as the one in the preceding sub-section, with obvious modifications. It is then tacitly assumed that the permeability is constant in the wire, i.e. unaffected by the variation in field strength over the wire cross-section area.

XII. Acknowledgment

Prof. Juan Carlos del Pino López (Universidad de Sevilla, Spain) is thanked for providing calculated results by the 3D FEM model, which was used as reference in this work. He is also thanked for clarifications regarding the geometry and modeling assumptions.

XIII. References

[1] J. Bremnes, G. Evenset, and R. Stølan, "Power loss and inductance of steel armored multi-core cables: Comparison of IEC values with 2.5D FEA results and measurements", in Proceedings of the CIGRÉ Session 2010, Paris, France, August 2010.

[2] R. Stølan and M. Hatlo, "Armor loss in three-core submarine cables - smeasurements of cable impedance and armor wire permeability", in Proceedings of the CIGRÉ Session 2018, Paris, France, August 2018.

[3] International Electrotechnical Commission. Electric Cables—Calculation of the Current; IEC 60287; IEC Press: Geneva, Switzerland, 2006.

[4] G. Bianchi and G. Luoni, "Induced currents and losses in single-core submarine cables", *IEEE Trans. Power Apparatus and Systems*, vol. 95, pp. 49-58, Jan/Feb 1976.

[5] J.S. Barret and G.J. Anders, "Circulating current and hysteresis losses in screens, sheaths and armor of electric power cables – mathematical models and comparison with IEC Standard 287, *IEE Proc. Sci. Meas. Technol.*, vol. 144, no. 3, pp. 101-110, May 1997.

[6] R. Benato, S. Dambone Sessa, M. Forzan, M. Marelli, and D. Pietribiasi, "Core laying pitch-long 3D finite element model of an AC three-core armored submarine cable with a length of 3 metres," *Electric Power Systems Research*, vol. 150, pp. 137–143, 2017.

[7] S. Sturm, A. Kűchler, J. Paulus, R. Stølan, and F. Berger, "3D-FEM modelling of losses in armored submarine power cables and comparison with measurements," in CIGRE´ Sessions, France, August 2020.

[8] J. C. del Pino-Lopez, M. Hatlo, and P. Cruz-Romero, "On simplified 3D finite element simulations of three-core armored power cables," *Energies*, vol. 11, no. 11, pp. 1–14, Nov 2018.

[9] J. C. Del-Pino-Lopez and P. Cruz-Romero, "Experimental validation of ultra-shortened 3D finite element models for frequency-domain analyses of three-core armored cables," *IEEE Trans. Power Delivery*, doi: 10.1109/TPWRD.2022.3158870.

[10] B. Gustavsen, M. Høyer-Hansen, P. Triverio, U.R. Patel, "Inclusion of wire twisting effects in cable impedance calculations", *IEEE Trans. Power Delivery*, vol. 31, no. 6, pp. 2520-2529, Dec. 2016.

[11] K.F. Goddard, J.A. Pilgrim, R. Chippendale, and P.L. Lewin, "Induced losses in three-core SL-type high-voltage cables", *IEEE Trans. Power Delivery*, vol. 30, no. 3, pp. 1505-1513, June 2015.

[12] C.H. Chien and R.W.G. Bucknall, "Harmonic calculations of proximity effect on impedance characteristics in subsea power transmission cables", *IEEE Trans. Power Delivery*, vol. 24, no. 4, pp. 2150-2158, October 2009.

[13] J.C. del Pino Lopez and P. Cruz-Romero, "A 3D parametric thermal analysis of submarine three-core power cables", *Renewable Energy and Power Quality Journal* (RE&PQJ), ISSN 2172-038 X, vol. no.18, pp. 363-368, June 2020.

[14] J. Weiss, and Z.J. Csendes, "A one-step finite element method for multiconductor skin effect problems", *IEEE Trans. Power Apparatus and Systems*, vol. 101, no. 10, pp. 3796-3803, October 1982.

[15] B. Gustavsen, A. Bruaset, J. Bremnes, and A. Hassel, "A finite element approach for calculating electrical parameters of umbilical cables", *IEEE Trans. Power Delivery*, vol. 24, no. 4, pp. 2375-2384, Oct. 2009.

[16] P. Pettersson and N. Schonborg, "Reduction of power system magnetic field by configuration twist," *IEEE Trans. Power Delivery*, vol. 12, no. 4, pp. 1678-1683, Oct. 1997.

[17] G.W. Brown and R.G. Rocamora, "Surge propagation in three-phase pipe-type cables, Part I – Unsaturated pipe", *IEEE Trans. Power Apparatus and Systems*, vol. 95, no. 1, pp. 89-95, Jan/Feb 1976.

[18] Y. Ivanenko, and S. Nordebo, "Estimation of complex valued permeability of cable armor steel", 2016 URSI International Symposium on Electromagnetic Theory (EMTS), 14-18 August 2016.

[19] A.P.S. Baghel, B. Sai Ram, L. Daniel, S.V. Kulkarni, G. Krebs, J.B. Blumenfeld, and L. Santandrea, "An alternative approach to model mechanical stress effects on magnetic hysteresis in electrical steels using complex permeability", *Computational Materials Science*, vol. 166, pp. 96-104, August 2019.

[20] M. Hatlo, E. Olsen, R. Stølan and J. Karlstrand, "Accurate analytic formula for calculation of losses in three-core submarine cables", Proc. 9th Int. Conf on Insulated Power Cables, Jicable'15, France, June 2015.

[21] W.G. Hurley and W.H. Wölfle, *Transformers and inductors for power electronics: Theory, design and applications*, John Wiley & Sons, 2013.

XIV. Biography

Bjørn Gustavsen (M'94–SM'2003–F'2014) was born in Norway in 1965. He received the M.Sc. degree and the Dr. Ing. degree in Electrical Engineering from the Norwegian Institute of Technology in Trondheim, Norway, in 1989 and 1993, respectively. Since 1994 he has been working at SINTEF Energy Research, currently as Chief Research Scientist. His interests include simulation of electromagnetic transients and modeling of frequency dependent effects. He spent 1996 as a Visiting Researcher at the University of Toronto, Canada, and the summer of 1998 at the Manitoba HVDC Research Centre, Winnipeg, Canada. He was Marie Curie Fellow at the University of Stuttgart, Germany, August 2001–August 2002. He is convenor of CIGRE JWG A2/C4.52.